J. Fluid Mech. (1990), *vol.* 219, *pp.* 313–336
Printed in Great Britain

Anomalous reflection of a shock wave at a fluid interface

By JOHN W. GROVE[1] AND RALPH MENIKOFF[2]

[1] Department of Applied Mathematics and Statistics, State University of New York at Stony Brook, Stony Brook, NY 11794, USA

[2] Theoretical Division, Los Alamos National Laboratory, Los Alamos, NM 87545, USA

(Received 8 March 1989 and in revised form 17 November 1989)

Several wave patterns can be produced by the interaction of a shock wave with a fluid interface. Regular wave patterns have previously been explained by a shock-polar analysis. We focus on an irregular wave pattern that typically occurs when a shock passes from a medium of high to low acoustic impedance. Curvature of either the shock front or contact causes the flow to bifurcate from a locally self-similar quasi-stationary shock diffraction, to an unsteady anomalous reflection. We show that the anomalous reflection wave pattern can be explained with a modified shock-polar analysis in which the geometric node velocity is replaced by a downstream boundary condition. Anomalous reflection is analogous to the transition from a regular to a Mach reflection when the reflected wave is a rarefaction instead of a shock. These bifurcations have been incorporated into a front-tracking code that provides an accurate description of wave interactions. Numerical results for two illustrative cases are described: a planar shock passing over a bubble, and an expanding shock impacting a planar contact.

1. Introduction

Wave patterns play a central role in understanding compressible fluid flow. In general two-dimensional flow consists of one-dimensional waves (shock, contact, or rarefaction) embedded in a smooth background flow. Elementary wave patterns are the local flow about the intersection of the one-dimensional waves. They are the most singular part of the solution to Euler's equations. The smooth background flow causes the elementary wave patterns to be quasi-steady (i.e., slowly varying in time) (Chern *et al.* 1985) or may cause them to bifurcate at discrete times (Grove 1989). In addition, the elementary wave patterns may interact causing them to scatter and bifurcate (Glimm & Sharp 1986). One well-known case is the transition between regular and Mach reflection. This can occur when a shock wave reflects off a curved wedge as the angle between the shock wave and wall increases.

A large number of wave patterns formed by the interaction of shock, contact, and rarefaction waves have been observed experimentally (see e.g., Jahn 1956; Abd-el-Fattah & Henderson 1978*a*, *b*; Ben-Dor, Dewey & Takayama 1987). Elementary wave patterns that can be explained by a shock-polar analysis are called regular. All others are called irregular.

The local structure of a regular wave pattern corresponds to a solution of a Riemann problem for a steady supersonic flow. We note that steady supersonic flow is described by hyperbolic partial differential equations. In two space dimensions, a regular wave pattern consists of two incoming waves that determine the initial data

for a Riemann problem, and three outgoing waves some of which may be degenerate. The point of intersection of these waves is called a node. The types of nodes that characterize these wave patterns have been classified according to the incoming waves by Glimm *et al.* (1985) into five categories: the diffraction of a shock wave at a fluid interface (diffraction node); the overtaking of one shock wave by another (overtake node); the collision of shock waves of opposite families (cross node); the splitting of a shock wave (Mach node); and the transmission of a shock through a fluid interface (transmission node).

An irregular wave pattern results from the breakdown in the local description of an elementary wave pattern in terms of steady supersonic flow. This may occur for two reasons. First, with respect to the frame of reference of the node a stationary oblique shock may result in a transonic flow. As a result the steady flow equations are of mixed hyperbolic–elliptic type. Second, a solution to the Riemann problem may fail to exist. This is because the shock polars are bounded curves and may not intersect. Irregular wave patterns typically result from the bifurcation of a regular wave pattern into a composite of other elementary wave patterns. This occurs when the flow behind an oblique shock becomes sonic. For example consider an incident shock reflecting off a contact (Henderson 1988). The transition from regular to Mach reflection corresponds to a diffraction node bifurcating into a Mach node and a transmission node. This occurs when the flow behind the reflected shock becomes sonic.

In general, interactions between shock waves and contact discontinuities can be divided into two classes, slow–fast or fast–slow depending on whether the shock is incident in the material with lower or higher acoustic impedance respectively. In the slow-fast case when the flow behind the transmitted shock becomes sonic a precursor wave pattern develops. In the fast-slow case when the flow behind the incident shock becomes sonic a pattern with reflected rarefactions analogous to a Mach reflection develops.

In this paper we discuss the mathematical formulation of the elementary wave patterns. A regular wave pattern is described as a solution to a Riemann problem for two-dimensional steady supersonic flow. The non-existence of the solution to this Riemann problem leads to the irregular wave patterns. In particular we analyse an irregular wave pattern called anomalous reflection. It is named after an important application. Namely, in the description of an underwater detonation this node leads to an anomalously low pressure near the surface of the water. Anomalous reflection commonly occurs when the regular wave pattern for the reflection of a shock from a contact bifurcates in the fast–slow case. This bifurcation is the analogue of the transition from regular to Mach reflection when the reflected wave is a rarefaction instead of a shock.

The bifurcation from a diffraction node with a reflected rarefaction to an anomalous reflection node may occur when either or both of the incident shock wave and fluid interface are curved. Measured in the frame in which the node is stationary the Mach number of the state immediately behind the incident shock wave decreases as the angle between the two incoming waves increases. When the flow behind the incoming shock at the node becomes sonic, the leading edge of the reflected rarefaction splits off from the node and begins to overtake the incident shock. Further increase in the angle between the incoming shock and contact leads to a second bifurcation in which the trailing edge of the reflected rarefaction also splits off from the node. This wave pattern is analogous to a Mach configuration; the portion of the incident shock between the contact and the leading edge of the rarefaction

corresponds to the Mach stem and the non-centred rarefaction corresponds to the reflected wave. This non-centred reflection is necessary because a Mach configuration with a centred reflected rarefaction is prohibited by two-dimensional shock stability (Menikoff & Plohr 1989).

Anomalous reflection is particularly important in two applications: a shock passing over a bubble, and an underwater explosion. In both cases the angle between the incoming shock and the contact varies. In the first case there is a planar shock and a curved contact. In the second case the contact is planar and the shock is curved. To illustrate how the anomalous reflection node occurs in the context of real fluid flows the solutions for both examples are calculated using a front tracking code. The results of these simulations are presented and discussed.

2. Mathematical formulation

2.1. *The equations of motion*

Let us consider an ideal fluid for which we can neglect viscosity, heat conduction and radiation. The evolution of the fluid is governed by the Euler equations describing the conservation of mass, momentum, and energy (see e.g. Landau & Lifshitz 1959):

$$\partial_t \rho + \nabla \cdot (\rho \boldsymbol{q}) = 0, \tag{2.1a}$$

$$\partial_t (\rho \boldsymbol{q}) + \nabla \cdot (\rho \boldsymbol{q} \otimes \boldsymbol{q}) + \nabla P = 0, \tag{2.1b}$$

$$\partial_t (\rho \mathscr{E}) + \nabla \cdot (\rho (\tfrac{1}{2} q^2 + H) \boldsymbol{q}) = 0, \tag{2.1c}$$

where ρ is the mass density, $\boldsymbol{q}$ is the particle velocity ($q = |\boldsymbol{q}|$), $\mathscr{E} = \frac{1}{2}q^2 + E$ is the total specific energy, E is the specific internal energy, P is the pressure, $H = E + PV$ is the specific enthalpy, and $V = 1/\rho$ is the specific volume. The equilibrium thermodynamic pressure P is given by a function $P = P(V, E)$ referred to as the equation of state. This function describes the thermodynamic properties of the fluid.

To study wave interactions it is useful to consider Riemann problems. A Riemann problem is an initial-value problem for a hyperbolic systems of conservation laws (such as system (2.1) with scale-invariant initial data. In two space dimensions this implies that there is a point about which the values of the initial data are constant along rays. We are interested in the wave patterns that occur when the distinguished point corresponds to the intersection of two incoming one-dimensional waves, i.e. data that correspond to the interaction of a pair of waves that are either shocks or contact discontinuities. Since both the Cauchy data and the evolution equations are scale invariant, the solution to the Riemann problem is also scale invariant. This means that the equations can be reduced to those for pseudo-steady flow. The local singularity structure of an elementary wave pattern is determined by further reducing the equations to those for steady flow.

2.2. *Scale-invariant two-dimensional flow*

Let u and v be the x- and y-components of the velocity. For two-dimensional flow we choose the z-component of the velocity to be zero.

2.2.1. *Pseudo-two-dimensional flow*

Pseudo-steady flow is described in terms of the scaled coordinates $\xi = x/t$ and $\eta = y/t$, and the pseudo velocity $\tilde{\boldsymbol{q}}$ with components $\tilde{u} = u - \xi$ and $\tilde{v} = v - \eta$. When the variables depend on x, y, and t only through the scaled coordinates ξ and η, the

system (2.1) reduces to (see e.g. Jones, Martin & Thornhill 1951 or Chang & Hsiao 1989)

$$(\rho\tilde{u})_\xi + (\rho\tilde{v})_\eta = -2\rho, \tag{2.2a}$$

$$(\rho\tilde{u}^2 + P)_\xi + (\rho\tilde{u}\tilde{v})_\eta = -3\rho\tilde{u}, \tag{2.2b}$$

$$(\rho\tilde{u}\tilde{v})_\xi + (\rho\tilde{v}^2 + P)_\eta = -3\rho\tilde{v}, \tag{2.2c}$$

$$(\rho\tilde{u}(\tfrac{1}{2}\tilde{q}^2 + H))_\xi + (\rho\tilde{v}(\tfrac{1}{2}\tilde{q}^2 + H))_\eta = -2\rho(\tilde{q}^2 + H). \tag{2.2d}$$

This system is hyperbolic when the pseudovelocity is supersonic, i.e. the Mach number $\tilde{M} = \tilde{q}/c$ is greater than one, where c is the sound speed. (See e.g. Courant & Friedrichs 1948.) The streamlines or particle trajectories define the time-like direction. The hyperbolic modes consist of two families of acoustic waves and two linearly degenerate modes. The characteristic speed of the waves corresponds to a direction in the (ξ, η)-plane. Let $\tilde{\theta}$ and $\tilde{q}$ be the polar coordinates of the velocity $\tilde{\boldsymbol{q}}$. The acoustic modes have characteristic directions with polar angles $\tilde{\theta} \pm \tilde{A}$ where the Mach angle $\tilde{A}$ is given by $\sin \tilde{A} = \tilde{M}^{-1}$. Both degenerate modes are directed along the particle trajectory. A wave belonging to the degenerate family is a contact discontinuity plus a vortex sheet across which the pressure and $\tilde{\theta}$ are continuous while the other variables may have jumps. When the pseudovelocity is subsonic, system (2.2) is of mixed type. The linearly degenerate modes remain hyperbolic and the acoustic modes become elliptic.

Let $\tilde{\boldsymbol{r}} = (\xi, \eta)$, and $\tilde{r} = |\tilde{\boldsymbol{r}}|$. For physical initial conditions (q and c finite), $\tilde{r}/M \to c$ as $\tilde{r} \to \infty$. Hence the pseudo-steady equations are asymptotically hyperbolic. Furthermore, on a circle of sufficiently large radius $\tilde{r}$, corresponding to a small fixed t, all the characteristics are directed inward and the circle can serve as a boundary on which to specify data for the initial-value problem. The number of independent variables in two-dimensional pseudo-steady flow (ξ and η) and a one-dimensional flow (x and t) are the same. Many features of the wave structure for the two systems are similar. We note that the source terms in the pseudo-steady flow have a similar effect to those which occur for one-dimensional flow in cylindrical or spherical geometry. However, the initial-value problem for two-dimensional pseudo-steady flow is in general more complicated. Here the manifold on which the initial data is specified is closed and bounded, which can lead to the formation of a free elliptic boundary within the domain. This elliptic region is needed to regularize the singularity that would occur from the convergence of the characteristics emanating from the initial manifold. Unlike a hyperbolic equation, which is evolutionary in nature, the free boundary results in the initial-value problem having features in common with an eigenvalue problem. The elliptic boundary arises when oblique transonic shocks occur. Thus, even though near the initial manifold the problem is hyperbolic, it is in general of mixed hyperbolic–elliptic type.

Pseudo-steady flows are observed for example when a shock wave impacts a wedge or diffracts around a corner. Experiments show that the solution to the two-dimensional Riemann problem may result in several diverging elementary wave patterns; e.g. a shock wave impinging on a wedge leading to double Mach reflection (Ben-Dor & Glass 1979), or the diffraction of a shock around a concave corner (Skews 1967). An elementary wave pattern is the local wave pattern consisting of the intersection of two incoming one-dimensional waves plus up to three outgoing waves and is the leading singularity in the solution to the fluid flow equations. We call the intersection of waves which form an elementary wave pattern a node. The different nodes are connected by one-dimensional waves and surrounded by a smooth background flow. This is the analogue to one-dimensional flow in which an initial

discontinuity (one-dimensional Riemann problem) is resolved into several elementary waves (shock, contact, or rarefaction) connected by constant states.

The local structure about a node is determined by the solution for small values of the pseudo-steady variables. When ξ and η are small, the source terms in the pseudo-steady flow equations are unimportant. Small ξ and η correspond in the full time-dependent two-dimensional problem to large values of t. As a result the elementary wave patterns are asymptotic solutions for large t and hence the solution to the one-dimensional Riemann problem for the equations of steady two-dimensional flow. These elementary wave patterns are determined by shock-polar relations. The source terms in the pseudo-steady flow equations result in the elementary wave patterns being quasi-steady, i.e. the elementary wave patterns slowly vary in time.

There is a helpful analogy between the elementary wave patterns in two-dimensional flow and shock waves in one-dimensional flow. Smooth spatial variations in one-dimensional flow cause a time variation in the strength of a shock wave. Yet at any instant in time the states across the discontinuity satisfy the Hugoniot relations for a steady wave. Similarly, smooth spatial variations in two-dimensional flow cause an elementary wave pattern to vary in time. But at any instant of time the discontinuities from the intersection of the one-dimensional waves satisfy the shock polar relations for a steady elementary wave pattern. Thus, the Hugoniot relations and the shock polar relations express the local conservation laws for discontinuities in one and two dimensions respectively.

2.2.2. *Steady two-dimensional flow*

For steady two-dimensional flow the equations of motion are obtained by setting the time derivatives to zero. The system (2.1) reduces to

$$(\rho u)_x + (\rho v)_y = 0, \tag{2.3a}$$

$$(\rho u^2 + P)_x + (\rho uv)_y = 0, \tag{2.3b}$$

$$(\rho uv)_x + (\rho v^2 + P)_y = 0, \tag{2.3c}$$

$$(\rho u(\tfrac{1}{2}q^2 + H))_x + (\rho v(\tfrac{1}{2}q^2 + H))_y = 0. \tag{2.3d}$$

Steady wave patterns are observed for example in wind-tunnel experiments.

With the correspondence $x \leftrightarrow \xi, y \leftrightarrow \eta, u \leftrightarrow \tilde{u}$ and $v \leftrightarrow \tilde{v}$ the mathematical structure of the steady equations is the same as the pseudo-steady equations except that the source terms are 0. In particular, the steady equations are hyperbolic for supersonic flow.

Let us consider an elementary two-dimensional wave pattern. The incoming (outgoing) waves are adjacent to the upstream (downstream) flow and their wave type corresponds to a characteristic pointing towards (away from) the node. For a shock (rarefaction) wave the streamlines are bent towards (away from) the node for an incoming wave and away from (towards) the node for an outgoing wave. Incoming waves, which may be either shocks or contact discontinuities, bend the upstream particle trajectories towards each other and are the cause of the interaction. Outgoing waves bend the downstream particle trajectories to be parallel to each other and are the result of the interaction. When the flow behind the incoming waves is supersonic in the frame of the node, the incoming waves specify the initial conditions for a Riemann problem of the steady two-dimensional flow equations. The particle trajectories are the time-like direction. If the solution to the Riemann problem exists and the flow is entirely supersonic it determines an elementary wave

pattern corresponding to a regular node. In this case the outgoing waves are completely determined by the upstream data.

The solution to the Riemann problem of the steady equations is complicated by the fact that the type of the PDEs (hyperbolic or mixed) depends on the nature of the flow (supersonic or transonic). When the flow is transonic and the equations are of mixed type the solution to the Riemann problem may not exist or not be unique. The steady solution is in the frame of the node. Thus, for a given pair of incoming waves in the laboratory frame, it is important to determine the node velocity in order to know the equation type. For a regular node, the node velocity is determined geometrically from the wave speeds of the incoming waves and the angle between them.

An irregular wave pattern occurs when the Riemann problem for two-dimensional steady flow fails to have a regular solution. In this case, some downstream information must be used together with the incoming waves to determine the wave pattern. It is helpful to think about the flow physically by considering what happens when a regular wave pattern is perturbed by increasing the angle between the incoming waves while leaving their strength fixed. In the frame of the node when one of the one-dimensional waves (either incoming or outgoing) becomes sonic the wave pattern bifurcates. Intuition for the bifurcations come from experimental studies of the interaction of a shock on a contact (diffraction node) leading to outgoing waves consisting of a transmitted shock, a contact and a reflected shock or rarefaction (Jahn 1956; Henderson 1988). Which wave becomes sonic first depends on the relative wave impedances across the contact. For weak shocks the wave impedance is approximately the acoustic impedance (ρc). In general the wave impedance is $\rho\sigma$, where σ is the wave speed and depends on the strength of the shock (Henderson 1989). In the slow–fast case the transmitted shock becomes sonic and a precursor develops in the transmitted medium, leading the node to split into a composite of several nodes (Abd-el-Fattah & Henderson, 1978*b*). The reflected shock becoming sonic corresponds to the transition between regular and Mach reflection for steady flow (the transition criterion is more complicated for pseudo-steady flow) (Hornung 1986). The fast–slow case when the incident shock becomes sonic is discussed in this paper.

2.3. *Regular wave patterns*

A regular wave pattern corresponds to a solution of a Riemann problem for a steady supersonic two-dimensional flow. The initial state is determined by the collision of two incoming waves: shock on shock, or shock on contact. The solution to the Riemann problem consists of two outgoing non-degenerate waves of the opposite families, shock or rarefaction, separated by a contact discontinuity. A steady two-dimensional shock is an oblique shock and a rarefaction is a Prandtl–Meyer fan. A contact may also be vortex sheet, i.e. the tangential velocity may be discontinuous across the contact. This corresponds to the two degenerate hyperbolic modes. Thus, in general a regular wave pattern corresponds to the intersection of five waves; two incoming and three outgoing. The qualitative structure of the solution to a steady two-dimensional Riemann problem is analogous to the solution to a Riemann problem for one-dimensional flow. The outgoing waves are determined by the intersection of the projection of wave curves; for one-dimensional flow the projection is in the (P, u)-plane, and for two-dimensional steady flow the projection is in the (P, θ)-plane.

There are several important differences between Riemann problems for steady two- and one-dimensional flow (Menikoff 1989). In particular, the wave curves have

different properties. For physically reasonably equations of state the one-dimensional wave curve is monotonic and unbounded. This results in the existence and uniqueness of a solution to the one-dimensional Riemann problem (Menikoff & Plohr 1989). The steady two-dimensional wave curves are closed and bounded. As a result the solution to the steady two-dimensional Riemann problem may not be unique or may not exist. There is a further difficulty since one is usually interested in a flow observed in a frame that is moving with respect to the wave interactions. Thus, there is the problem of determining the Galiean transformation from this 'lab' frame into the frame in which the node is stationary.

2.3.1. *Supersonic steady-state wave curves*

We next describe the wave curves for supersonic steady two-dimensional flow. Wave curves are parametrized by the initial state, ρ, E, and $\boldsymbol{q}$. There is a wave curve for each hyperbolic mode. The wave curve for a non-degenerate mode has two parts corresponding to shock and rarefaction waves. The portion of the wave curve corresponding to shock waves is called a shock polar.

A shock polar (Courant & Friedrichs 1948, §§117–122) is the locus of final states that can be connected to a given initial state by a stationary oblique shock wave. It is composed of two families, one corresponding to each sound mode. It is convenient to label the families by whether θ increases in the clockwise or counterclockwise direction as P is increased.

There is a one-to-one correspondence between stationary oblique shocks with a given incident Mach number and normal one-dimensional shocks. In particular suppose both the waves have initial state with density, energy and pressure ρ_0, E_0 and P_0 respectively. The thermodynamics states on either side of a shock wave are related by the Hugoniot equation

$$E = E_0 + \tfrac{1}{2}(P+P_0)(V_0 - V). \tag{2.4}$$

For a normal shock the wave speed with respect to the fluid ahead is $\sigma = V_0(-\Delta P/\Delta V)^{\frac{1}{2}}$, and the jump in the velocity across the shock is given by $u - u_0 = \pm\rho_0(V_0 - V_1)\sigma$. Similarly, for an oblique shock the angle with respect to the incoming streamline is $\beta = \sin^{-1}(\sigma/q_0)$, and the jump in the flow direction across the shock is given by (Grove 1989)

$$\tan(\theta - \theta_0) = \pm\left[\frac{P-P_0}{\rho_0 q_0^2 - (P-P_0)}\right]\cot\beta. \tag{2.5}$$

The flow velocities on either side of a stationary shock, normal or oblique, are related by Bernoulli's equation

$$\tfrac{1}{2}q^2 + H = \tfrac{1}{2}q_0^2 + H_0. \tag{2.6}$$

Despite the correspondence between one-dimensional shocks and two-dimensional oblique shocks there is an important qualitative difference between the one-dimensional shock Hugoniot and the two-dimensional shock polar. For most materials the projection of the one-dimensional shock Hugoniot in the (P, u)-plane is monotonic and semi-infinite. On the other hand oblique shocks on the shock polar are limited in strength by the incident Mach number. The projection of the shock polars for both families in the (P, θ)-plane forms a closed bounded loop. As a result wave curves for different initial states may fail to intersect leading to non-existence of a solution to the Riemann problem, or the wave curves may intersect more than once leading to non-uniqueness of the solution to the Riemann problem.

In addition, the downstream state of a stationary oblique shock may be either

subsonic or supersonic. On a shock polar the weak shocks are supersonic and the strong shocks are transonic. Thus, while the shock polar may be the natural definition for the shock portion of the wave curve, the states on the shock polar are not entirely within the supersonic domain necessary for the steady equations to be hyperbolic. With reasonable conditions on the equation of state, the sound speed on the one-dimensional shock Hugoniot is monotonic and there is only one sonic point on each family of the shock polar. Furthermore, for two-dimensional shock stability the pressure at the sonic point is less than the pressure when θ is maximum (Menikoff & Plohr 1989). Thus, the supersonic portion of the shock polar is monotonic and bounded. As a result there can be at most one solution of the steady two-dimensional Riemann problem in which the flow remains supersonic and the equation are entirely hyperbolic. Non-existence and non-uniqueness of solutions to steady two-dimensional Riemann problems are the result of transonic oblique shocks.

There is also a one-to-one correspondence between a Prandtl–Meyer fan and one-dimensional rarefactions. In both cases the thermodynamic variables lie on an isentrope (constant entropy curve) determined by integrating the relation

$$\mathrm{d}E = -P\,\mathrm{d}V. \tag{2.7}$$

Along a one-dimensional rarefaction the velocity is determined by the partial Riemann invariant

$$u = u_0 \pm \int_{P_0}^{P} \frac{\mathrm{d}P}{\rho c}\bigg|_S. \tag{2.8}$$

Inside a Prandtl–Meyer wave the magnitude of the flow speed is found from Bernoulli's relation, (2.6), and the flow angle from the partial Riemann invariant (Thompson 1971)

$$\theta = \theta_0 + \int_{P_0}^{P} \mathrm{d}P \frac{\cos A}{\rho c q}\bigg|_S. \tag{2.9}$$

In analogy to the shock polar defined by (2.4)–(2.6) we shall refer to the locus of states defined by (2.7)–(2.9) as a rarefaction polar.

The wave curve for stationary supersonic flow through a given state with pressure P_0 is obtained by the concatenation of the branch of the shock polar with $P > P_0$ with the branch of the rarefaction polar with $P < P_0$. Standard theory (Lax 1957) shows that the combined curve is twice continuously differentiable. For a point on the wave curve, $\Delta\theta = \theta - \theta_0$ is called the turning angle of the wave. The incident flow must be supersonic for both an oblique shock and a Prandtl–Meyer fan to exist.

There is a useful analogy between steady two-dimensional wave patterns and time-dependent one-dimensional flow. With the streamline in the time-like direction, the wave pattern in two dimensions corresponds to the (x, t)-diagram in one dimension for the scattering of waves. The wave patterns and polar diagrams are described next.

2.3.2. *Elementary wave nodes*

In order to determine the wave pattern resulting from the interaction of two incoming waves it is first necessary to compute the node velocity. A geometric node velocity is defined as the phase velocity of the intersection point of the incoming waves when they are propagated in the normal direction with the appropriate one-dimensional wave speed. The first criterion for a regular wave pattern is that in the frame moving with the geometric node velocity the flow behind the incoming waves is supersonic. In this case the two states behind the incoming waves are the initial

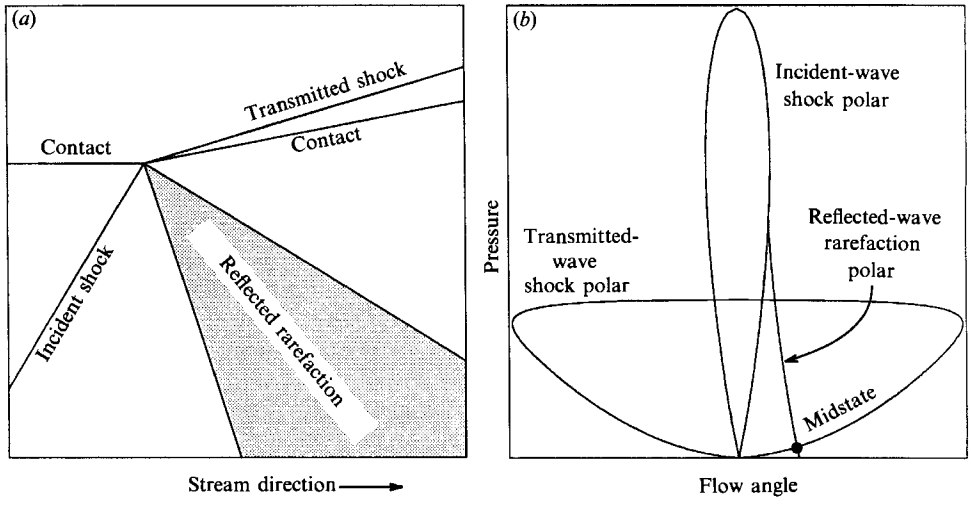

FIGURE 1. A sketch of the wave pattern and polar diagrams for a regular shock–contact diffraction that produces a reflected rarefaction wave.

conditions for a steady two-dimensional Riemann problem. The second criterion for a regular wave pattern is that there exists a solution of the Riemann problem. The solution to the Riemann problem is determined by the intersection of the projections in the (P, θ)-plane of the two wave curves for the initial states. The third criterion is that the flow behind the outgoing waves is compatible with the downstream boundary conditions. The wave curves have at most one intersection in which the flow behind the outgoing waves is supersonic. If the downstream boundary condition is that the flow is supersonic then the incoming waves completely determine an elementary wave pattern.

The common wave patterns have been discussed by Landau & Lifshitz (1959, §102), and classified by Glimm *et al.* (1985) and Henderson (1988). Here we refine and extend the classification of elementary wave patterns.

The regular wave patterns may be subdivided into three cases according to the incoming wave types. A diffraction node occurs when a shock impacts a contact. It results in a transmitted shock, a displaced contact, and a reflected wave. The reflected wave may be either a shock or a rarefaction. When the wave impedance is lower for the medium of the transmitted wave than for the medium of the incident shock the reflected wave is a rarefaction. There is a degenerate case in which the reflected wave has zero strength. Usually the flow behind the outgoing waves is supersonic but this is not true in general. A typical example of a diffraction wave pattern and polars for this case is sketched in figure 1.

An overtake node is produced when one shock wave overtakes another shock of the same family. It results in a transmitted shock, a displaced contact and a reflected wave that is either a shock or a rarefaction. The degenerate case when a shock is overtaken by a sonic signal (zero strength shock) is important in the analysis of the anomalous reflection. The collision of two shocks of the opposite families produces a cross-node. Here the scattered waves are shocks separated by a contact discontinuity.

There are two other common elementary nodes which can be constructed using wave curves. These differ from the previous regular nodes in that downstream data are needed in addition to the incoming waves to determine the node velocity. The first of these is the Mach node. A Mach node occurs for example when a regular

reflection bifurcates into Mach reflection. In a sense it is a degenerate case of a diffraction node in which the incoming contact has zero strength. The Mach node corresponds to one incoming shock splitting into two outgoing shocks separated by a contact. The flow behind one of the outgoing waves, the Mach stem, is always subsonic. This wave pattern corresponds to choosing the solution of the Riemann problem which is not entirely supersonic and shows that the non-uniqueness of the two-dimensional steady Riemann problem is physically important. For the anomalous node it is important to note that a Mach reflection with a reflected rarefaction cannot occur (Menikoff & Plohr 1989). This is because on the shock polar the pressure of the sonic point is below the pressure at the maximum turning angle. Furthermore, this is a necessary condition for two-dimensional shock stability.

The last common elementary wave pattern is a transmission node. It is similar to a degenerate diffraction node, i.e. no reflected wave. However, the incident shock is transonic in the frame of the node. This causes the equations for the flow behind the incoming waves to be of mixed type, hyperbolic–elliptic. Thus, even though this node can be described using wave curves, it does not correspond to a solution of a Riemann problem for the steady-state hyperbolic flow equations. The elliptic region is important for the stability of this node. For the quasi-steady time-dependent transmission node, the spatial dependence of the downstream flow is coupled to the node by the downstream boundary condition and causes the incident shock to curve. In contrast, a degenerate diffraction node is a transient state of a quasi-steady diffraction node as the reflected wave goes from a rarefaction to a shock or vice versa.

There is one more elementary wave pattern which can be determined with the use of wave curves. This is the kink node which is of important for compressible Kelvin–Helmholtz instability (Artola & Majda 1989). The kink node consists of an incoming rarefaction and outgoing shock separated by a combined vortex sheet and contact. There is a kink in the contact at the node. It is unusual in that the time-like directions are reversed across the contact. This is because in the frame of the node the vortex sheet is strong enough to reverse the directions of the particle trajectories on either side of the contact.

When any of the criteria for a regular wave pattern fail then the assumption of steady two-dimensional flow breaks down. In general one must consider the initial-value problem for pseudo-steady flow. However, there are cases when the local wave pattern can be constructed from a modified Riemann problem in which the node velocity is determined consistent with both the incoming waves and the downstream boundary data. An example of this is the anomalous reflection described in the next section.

3. Anomalous reflection

Many experiments have been performed to study the diffraction of a shock on a contact. Mach–Zehnder interferograms clearly show the changes in the wave pattern as the angle between an incident shock (with fixed strength) and a contact is varied. Many of the wave patterns have been explained using polar diagrams (Henderson 1966; Hornung 1986). One of the interferograms, figure 14(*g*) of Jahn (1956), shows an irregular wave pattern which corresponds to anomalous reflection. Jahn gave a qualitative description of this wave pattern. To quantitatively describe the anomalous reflection one must account for the variation of the node velocity resulting from the curvature of the incident shock. This affects the incident Mach number for the polar analysis.

3.1. *Physical description*

We begin by considering a diffraction node with a reflected rarefaction. Suppose the shock strength is held fixed as the angle between the incoming shock and contact is increased. The node velocity is determined from the shock velocity and the angle between the shock and contact as described above. In particular the node velocity decreases, and on the appropriate shock polar the incident shock goes from supersonic to subsonic. Because a Prandtl–Meyer fan can only exist for supersonic flow, a steady solution fails to exist and the diffraction node must bifurcate when the incident shock becomes sonic.

In this case a sound signal propagates out from the node causing the incident shock to curve. The curvature changes the node velocity in such a way that at the node the incident shock remains sonic. This can be thought of as the head of the centred rarefaction peeling off from the diffraction node and propagating along the incident shock. This weakens the incident shock and causes it to curve and consequentially the transmitted shock also curves. This configuration has the appearance of a quasi-steady diffraction node together with a non-centred rarefaction running along a curved incident shock. The change in wave pattern may be considered as a bifurcation of a diffraction node into a sonic diffraction node plus a degenerate overtake node which then move apart. By a sonic diffraction node we mean that the state behind the incident shock is sonic with respect to the node. The overtake node is degenerate in the sense that the overtaking shock is of zero strength, i.e. a sonic signal or Mach line. The wave pattern is analogous to an (x,t)-diagram in one space dimension of a rarefaction overtaking a shock (N-wave) which then scatters off a contact.

As the angle between the contact and incident shock continues to increase more of the rarefaction peels off the diffraction node; the non-centred rarefaction becomes stronger and the centred rarefaction becomes weaker. When the strength of the centred rarefaction shrinks to zero the diffraction node becomes degenerate (no reflected wave). There are two possibilities: either the incident shock shrinks to zero strength, or the incident shock become transonic leading to a transmission node.

The former case occurs when there is a large difference in the compressibility of the fluids, e.g. air–water interface. In this case as the centred rarefaction shrinks to zero, the strength of the incident shock also shrinks to zero. The incident shock becomes normal to the interface and the trailing edge of the non-centred rarefaction wave becomes parallel to the incident shock. Thus, the non-centred reflected rarefaction is the same strength as the incident shock. The flow near the diffraction node is to leading order a one-dimensional unsteady flow with a rarefaction wave overtaking a shock wave from behind.

The latter case occurs when there is a small difference in the compressibility of the fluids. In this case the shock polars for the materials on each side of the contact cross at the sonic point for the medium of the incoming shock. Further increasing the angle provides a continuous mechanism for generating a transmission node with transonic incoming shock in the rest frame of the node.

In either case, the resulting wave pattern is analogous to a Mach node with a reflected rarefaction. The portion of the incident shock wave between the contact and the leading edge of the non-centred reflected rarefaction corresponds to the Mach stem.

3.2. *Numerical implementation*

The qualitative discussion of the anomalous reflection in the previous section can be incorporated into a front-tracking code to give an enhanced resolution of the interaction.

The method of front tracking provides a means of gaining enhanced resolution of computational problems with discontinuities by directly incorporating analytic knowledge about the solution into the numerics (Glimm & McBryan 1985; Glimm *et al.* 1981; Chern *et al.* 1985; Glimm *et al.* 1985). Previous work (Grove 1989) described the tracking (two-dimensional) of a regular shock–contact diffraction node. A shock–contact diffraction node is propagated between time steps of increment Δt as follows. Let $\boldsymbol{p}_{00}$ be the position of the node at the start of the time step. The pair of incoming waves (the incident shock and material interface) are first propagated independently ignoring their interaction. Their intersection is the node position $\boldsymbol{p}_0$ at the end of the time step. This determines the node velocity $\boldsymbol{v} = (\boldsymbol{p}_0 - \boldsymbol{p}_{00})/\Delta t$. The polar analysis is performed in the rest frame of the node. We use the node velocity to transform to this frame. If the state behind the incident shock is supersonic, it together with the state on the opposite side of the material interface provide data for a supersonic steady-state Riemann problem. When the solution to the Riemann problem exists it defines a regular wave pattern. The outgoing tracked waves are then modified to incorporate this solution. The smooth background flow causes the strength of the incoming waves and the angle between them to slowly vary. As a result the node which locally describes the leading-order singularity at the intersection of the waves is quasi-steady. When the solution to the Riemann problem fails to exist the node must bifurcate.

If the state behind the incident shock becomes subsonic then the incoming waves no longer defines a valid steady-state Riemann problem and the node must also bifurcate. A bifurcation to an anomalous reflection occurs when on the previous time step the reflected wave is a Prandtl–Meyer wave. The first step in modelling this bifurcation is to propagate the leading edge of the reflected wave onto the incident shock. This is done as before, by finding the point of intersection $\boldsymbol{p}_1$ between the two propagated curves. If the reflected wave is untracked, it is recovered by calculating the characteristic through the old node position corresponding to the state behind the incident shock. It is assumed that at the beginning of the time step the flow is supersonic, so this characteristic is real. The leading edge of the reflected rarefaction moves with sound speed with respect to the fluid in the direction normal to this characteristic. If the leading edge of the Prandtl–Meyer wave is tracked, it is disconnected from the original diffraction node and a new overtake node corresponding to the oblique overtaking of a characteristic (zero-strength shock wave) with a shock wave of the same family is installed at $\boldsymbol{p}_1$.

We next determine the node velocity which fixes the frame of reference for a new Riemann problem that determines the diffraction node after the bifurcation. As the rarefaction expands onto the incident wave, the incident shock near the material interface is weakened. This causes the incident shock to curve, decreasing the node velocity. The new node velocity must be geometrically consistent with both the change in the wave speed of the shock and the change in the angle between the shock and the contact. In addition, for the portion of the reflected wave attached to the node to be a centred rarefaction the flow behind the incident shock at the node must be sonic. Thus, for an irregular node we must solve for the node velocity from the

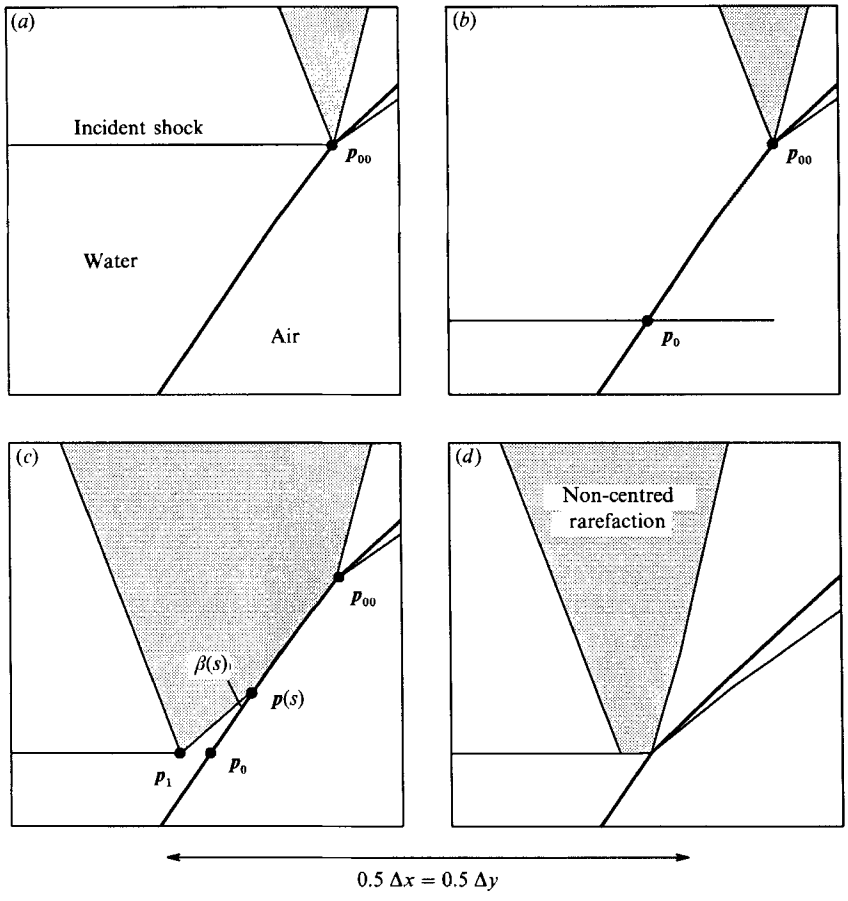

FIGURE 2. A diffraction node initially at $\boldsymbol{p}_{00}$ bifurcates into an anomalous reflection. The predicted new node position at $\boldsymbol{p}_0$ yields a Mach number of 0.984 behind the incident shock. The leading edge of the reflected Prandtl–Meyer wave breaks away from the diffraction node to form an overtake node at $\boldsymbol{p}_1$. The propagated position of the diffraction node is adjusted to return the flow to sonic behind the node.

downstream boundary condition before solving the Riemann problem. Then the solution is used to update both the incoming and outgoing waves.

It is convenient to use the propagated-node position instead of the corrected node velocity as an independent variable. We use arclength to parametrize the propagated material interface. Let $\boldsymbol{p}(s)$ be a point a distance s from point $\boldsymbol{p}_0$ when measured along the curve with the positive direction being oriented away from the node into the region ahead of the incident shock. Let $\beta(s)$ be the angle between the tangent vector to the material interface at $\boldsymbol{p}(s)$ and the directed line segment between the points $\boldsymbol{p}(s)$ and $\boldsymbol{p}_1$, see figure 2. Moving the node to position $\boldsymbol{p}(s)$, results in a node velocity $\boldsymbol{v}(s) = (\boldsymbol{p}(s) - \boldsymbol{p}_{00})/\Delta t$. Let $\boldsymbol{q}(s)$ be the velocity of the flow ahead of the incident shock in the frame that moves with node velocity $\boldsymbol{v}(s)$. The mass flux across the incident shock that makes an angle $\beta(s)$ with the upstream material interface is given by

$$m(s) = \rho_0 |\boldsymbol{q}(s)| \sin\beta(s). \tag{3.1}$$

Using the mass flux is equivalent to enforcing the consistency between the node

velocity and the incident wave geometry. It is numerically more stable than using the wave speed. The state behind the shock and hence its Mach number $M(s)$ are determined by $m(s)$ and the state ahead of the incident shock through the Hugoniot relations for an oblique shock. The new node position $\boldsymbol{p}(s_*)$ is determined by solving for s_* the nonlinear equation $M(s_*) = 1$. Finally, the state behind the incident shock with mass flux $m(s_*)$ together with the state on the opposite side of the contact are used as data for a steady-state Riemann problem. The solution determines the propagated or updated node. The state at the node serves as a boundary condition for the tangential sweep along the front. This enables information about the non-centred rarefaction originating at the node to propagate outward and weaken the incident shock causing it to curve.

The subsequent propagation of the anomalous reflection node is performed in the same way. The bifurcation simply repeats itself as more of the reflected rarefaction propagates up the incident shock. The leading edge of the reflected rarefaction wave that connects to the diffraction node is not tracked after the first bifurcation.

Secondary bifurcations occur when the trailing edge of the rarefaction overtakes the incident shock. These are detected in a couple of ways. If the incident shock is sufficiently weak, i.e. the normal shock Mach number is close to 1, then it is possible for the numerically calculated upstream Mach number to be less than one. Physically of course the state ahead of the incident shock is always supersonic, but if it is nearly sonic such numerical undershoot may occur. When this happens, the construction described above must be modified. The tracked trailing rarefaction edge is disengaged from the diffraction node and installed in a new overtake node found by intersecting the propagated characteristic with the ahead shock. The residual shock strength for the portion of the incident shock behind the rarefaction wave is small. The diffraction node at the material interface reduces to the degenerate case of a sonic signal diffracting through a material interface, and the induced downstream waves are also sound waves. It is convenient and more stable to consider degenerate nodes with a zero-strength incident wave rather than having a shock start or end in an interior region of the flow.

The second way in which the secondary bifurcation is detected occurs when the trailing edge of the rarefaction overtakes the shock. When this happens a new intersection between the incident shock and the trailing-edge characteristic is produced. Again the tracked characteristic is disengaged from the diffraction node and a new overtake node is installed at the point of intersection. Here, the residual shock strength behind the rarefaction is positive. The diffraction at the material interface is non-trivial and will produce an additional expansion wave behind the original one. Most often this new expansion wave is not tracked.

4. Planar shock passing over a bubble

One class of applications where the anomalous reflection is important is in flows where a shock passes over an inhomogeneity of lower wave impedance. The inhomogeneities are a source for generating turbulence and hot spots. Shock wave interactions with bubbles have been studied experimentally (Hass & Sturtevant 1987; Dear & Field 1988). Moreover, the propagation of the lead shock front over a bubble has been calculated numerically by Schwendeman (1988) using Whithams shock dynamics. Shock dynamics is an approximation to the fluid equations for the lead shock wave in which the interior flow is neglected. By contrast front tracking is a method for the solution of the fluid equations. It determines the reflected waves

and the interior flow as well as the lead shock. Most important, front tracking accounts for the coupling between the interior flow and shock waves. In addition, numerical calculations with shock-capturing methods are described in Picone & Boris (1988) and Winkler *et al.* (1987). There, interest is in the vorticity generation in the late stage after the shock has swept over the bubble. By contrast we are interested in the wave patterns and bifurcations that occur in the early stage as the shock interacts with the bubble.

Our first numerical example is the flow of a planar shock in water over a cylindrical air cavity. The water is treated with a stiffened gas equation of state

$$P(V,E) = \Gamma_0 \rho(E - E_\infty) - (\Gamma_0 + 1) P_\infty, \tag{4.1}$$

with $\Gamma_0 = 6$, $E_\infty = 0$, and $P_\infty = 3000$ atm. The air is treated as a polytropic gas

$$P(V,E) = (\gamma_0 - 1)\rho E, \tag{4.2}$$

with $\gamma_0 = 1.4$. For the unperturbed state $P_0 = 1$ atm, and the initial densities are $\rho_{\text{water}} = 1$ g/cc and $\rho_{\text{air}} = 0.0012$ g/cc. We note that this is a more extreme range of parameters, density and compressibility ratio, for the bubble and surrounding medium than previous calculations. Two cases with different initial water shock strengths are computed.

4.1. *Weak shock*

In the first case, the strength of the initial water shock is $P_{\text{shock}}/P_0 = 100$. The Mach number ahead of the shock is $M = u_s/c_{\text{water}} = 1.009$. Because of the large ratio of acoustic impedances $(\rho c)_{\text{water}}/(\rho c)_{\text{air}} \approx 3500$ and the stiff equation of state for water, the impedance match when the shock first hits the contact results in the water surface blowing into the air cavity with velocity u approximately twice that of the fluid velocity u_0 behind the original incident shock. As a consequence, the pressure behind the reflected rarefaction in the water is only slightly greater (about 6%) than P_0, and the transmitted shock in the air is very weak $u/c_{\text{air}} = 0.04$. Because the particle velocity is small relative to the shock velocity in both the air and water, the wave propagation is in the acoustic limit.

A time sequence of front plots is shown in figure 3. When the shock first hits the bubble, figure 3(*b*), a pair of diffraction nodes is formed. The rarefaction is very narrow because the Mach number of the incident shock in the water is small. Both the leading and trailing edge of the rarefaction are tracked. They lie within 1 zone of each other. The spreading is small because the characteristic velocity of the head and tail of the rarefaction are both $u + c \approx c_0$. Thus, the thin rarefaction has the appearance of a 'rarefaction shock'. The curvature of the bubble causes the angle between the incident shock and contact to increase and eventually each diffraction node bifurcates into an anomalous reflection. Subsequently, there is a second bifurcation into an anomalous Mach reflection as described above, figure 3(*c*). At this point, the shock at the bubble interface is reduced to zero strength. Finally, when the shock passes the back of the bubble, the two nodes formed by the diffraction of the zero-strength shock (Mach line) through the bubble interface coalesce and the water shock detaches from the bubble, figure 3(*d*). Because of the boundary conditions the expanding rarefaction passes out of the computational domain. The water–air contact moves very little during the time it takes the water shock to pass over the air bubble because the shock is very weak, $u_{\text{particle}} \ll u_{\text{shock}}$. Another consequence of the weak incident shock is that the transmitted shock in the air is a circle with a centre displaced from the cavity. This follows because the weak air shock has an almost constant wave speed (sound speed), and because of the large phase velocity

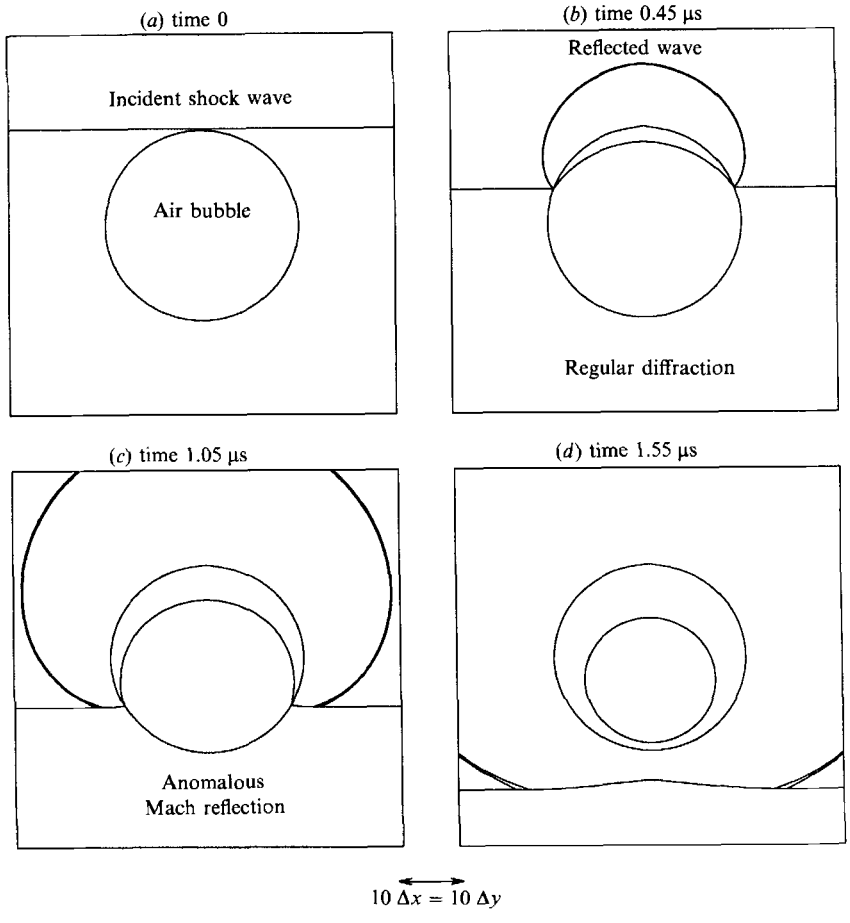

FIGURE 3. The production of an anomalous 'Mach' reflection. A shock wave with behind pressure of 100 bars (Mach number 1.009) in water is incident on a bubble of air. The upstream states are ambient at 1 atm. and standard densities. In one microsecond the trailing edge of the reflected Prandtl–Meyer wave has overtaken the incident shock producing an analogue to an ordinary Mach reflection where the reflected wave is a non-centred rarefaction. The grid is 60×60.

(shock speed water/shock speed air $\gg 1$) the air shock is almost normal to the contact.

The fronts move through an underlying Eulerian grid. They provide boundary conditions for each interior-connected component. In addition, smooth waves from the interior are coupled to and affect the propagation of the fronts. The interior grid provides information on the flow behind the fronts. A time sequence of pressure contours is shown in figure 4. Owing to the divergence of the flow there is an expansion wave behind the tail edge of the rarefaction. This causes the rarefaction to weaken. It also affects the time dependence of the nodes.

4.2. *Strong shock*

For the second case, the shock in the water is stronger, $P/P_0 = 10000$. The front plots are shown in figure 5 (compare with Schwendeman 1988, figure 11*b*). The nonlinearities of the flow are larger and the rarefaction spreads out over a larger distance. The anomalous reflection with the curvature of the incident shock is more

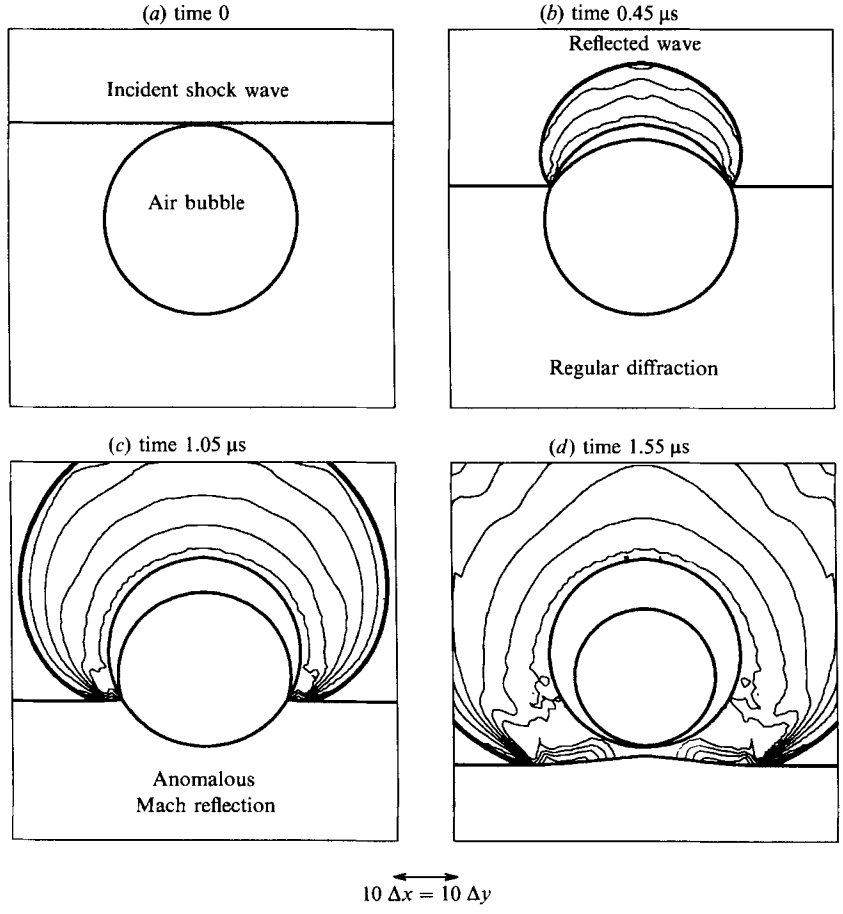

FIGURE 4. Pressure contours for figure 3. The contours are plotted on a scale of 0–100 bars. The tracked fronts are shown as a dark line superimposed on the pressure contours.

clearly visible, figure 5(*c*). The two phases of the bifurcation are also more distinct, figures 5(*c*) and 5(*d*). Furthermore, the contact is distorted because of the smaller ratio of wave speeds. A time sequence of pressure contours is shown in figure 6. Both the centred and non-centred rarefaction at the anomalous node is clearly seen, figure 6(*c*). At late time a jet from the front impacts the back of the contact resulting in a large pressure. In heterogeneous high explosives this mechanism is an important source of hot spots and has an important effect on the initiation and propagation of a detonation wave (Mader 1965).

5. Interaction of expanding shock on planar contact

Another class of application for which anomalous reflection is important occurs in flows when an expanding shock impacts a planar fluid surface. An important example of this is when the blast wave from an underwater explosion reaches the surface (Holt 1977). Irregular reflections at the water surface have been observed in numerical calculations, see e.g. Kamegai (1986). However, lack of resolution has smeared out and distorted the interaction, limiting the understanding of the wave pattern. Front tracking is well suited to this type of problem. Our second numerical

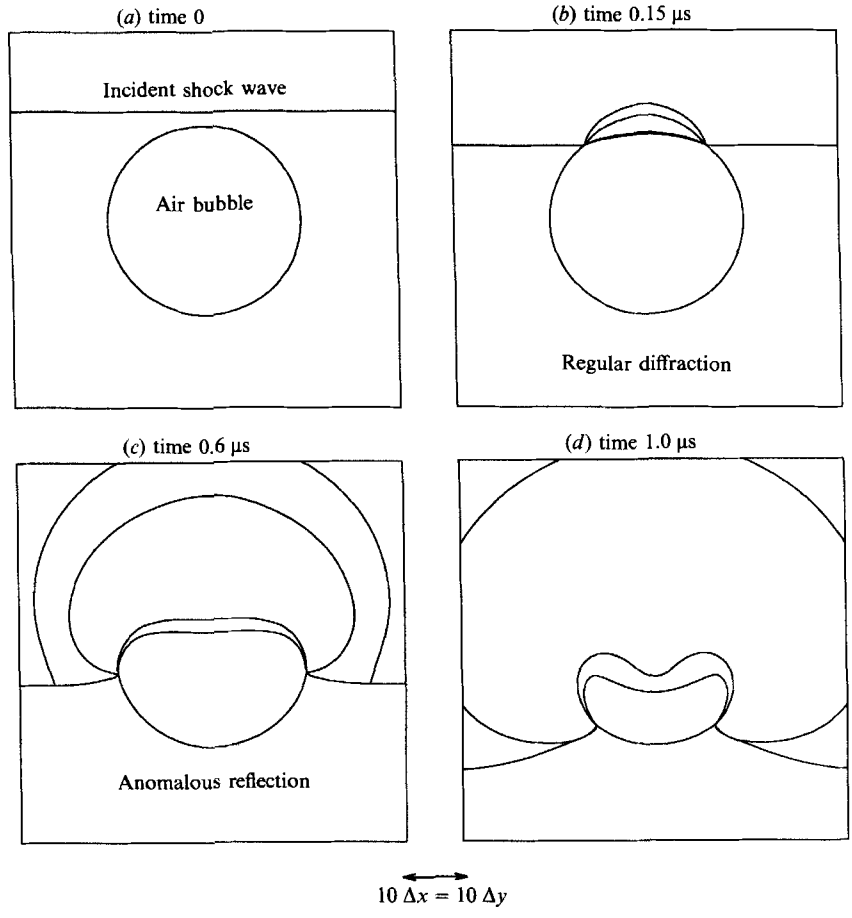

FIGURE 5. The collision of a shock wave in water with an air bubble. The fluids ahead of the shock are at normal conditions of 1 atm. pressure, with the density of water 1 g/cc and air 0.0012 g/cc. The pressure behind the incident shock is 10 Kbar with a shocked water density of 1.195 g/cc. The grid is 60×60.

example is a simulation of the flow resulting from an underwater detonation; a cylindrically expanding shock in water impacts the surface with air.

The detonation is modelled by a cylinder of reacting products at high energy density and pressure. For the reaction products, we used a polytropic equation of state with $\gamma = 1.4$, and initial density, $\rho = 1.25$ g/cc, and pressure, $P = 10$ Kbar. The initial conditions outside of the shock are at one atmosphere (≈ 1 bar) pressure and standard densities for air and water.

The first calculation begins with the reacting products slightly inside an expanding water shock having a radius of 1 m at a depth 2 m below the surface of the water. The velocity of the reaction products was set to match that of the fluid behind the water shock. The computational limit for the simulation cell is 80×80 m, and the grid is 150×150.

A time sequence of tracked fronts is shown in figure 7. Because gravity is unimportant on the timescale of the calculation, the initial water shock is still circular when it reaches the surface, figure 7(*b*). At this point a pair of diffraction nodes is formed and propagates along the interface in opposite directions. A

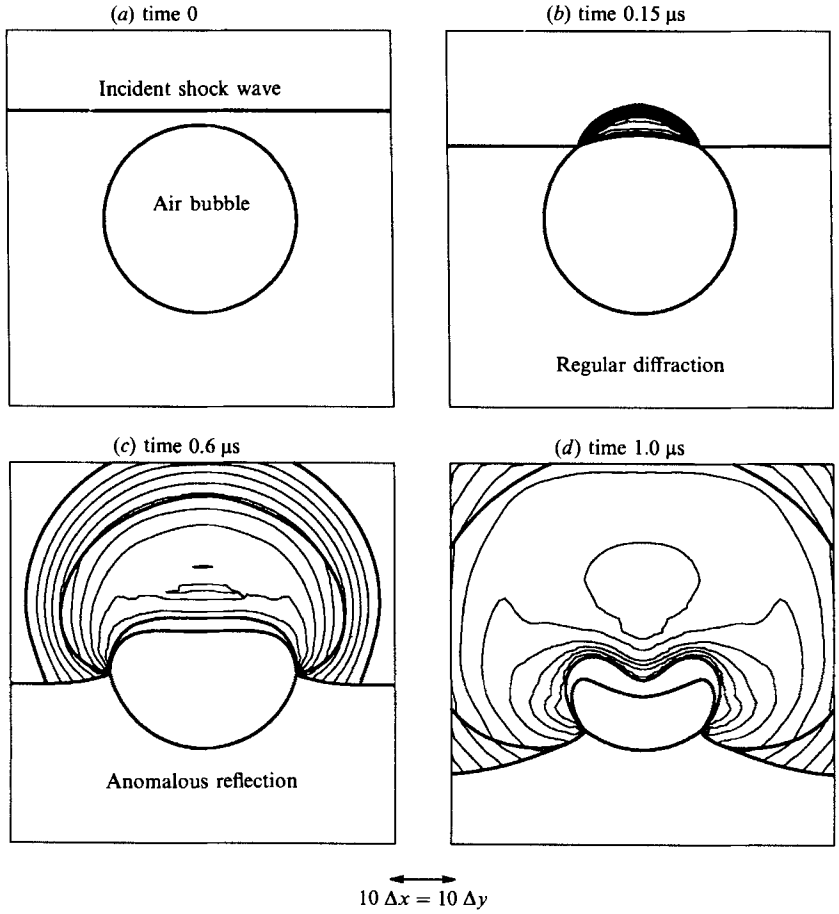

FIGURE 6. Contours of $\log(1+P)$ for figure 5. The contours in (*b*) and (*c*) are plotted on a scale of 0.001–10 Kbars, while the pressure range in (*d*) is 0–8.5 Kbars. The tracked fronts are shown as a dark line superimposed on the pressure contours.

transmitted shock propagates into the air and the reflected rarefaction in the water. When the water rarefaction reaches the reaction products, the release in pressure causes the bubble of reaction products to rise. When the bubble of reaction products approaches the surface, the rapid and asymmetric change in pressure distorts the shape of the bubble. The expanding water shock causes the angle between the shock and the contact to increase which results in a bifurcation to an anomalous reflection, figure 7 (*b*). This is seen in the pressure contours, figure 8. The shock speed of the expanding wave in the air slows at a larger rate than the shock speed of the water and falls behind. This leads to a precursor shock in the air ahead of the cylindrically expanding wave, figure 7 (*d*). The kink in the shock fronts at the interaction of the precursor and the expanding wave is indicative of a Mach configuration. The reflected wave for this configuration is not being tracked but is taken account by the interior scheme.

A second series of frames for the same interaction with a different set of parameters is shown in figure 9. Here, the initial shock is located 10 m below the water surface with an initial radius of 1 m. The parameters outside of the expanding shock are the same as in the previous calculation, but in this case the pressure behind the initial

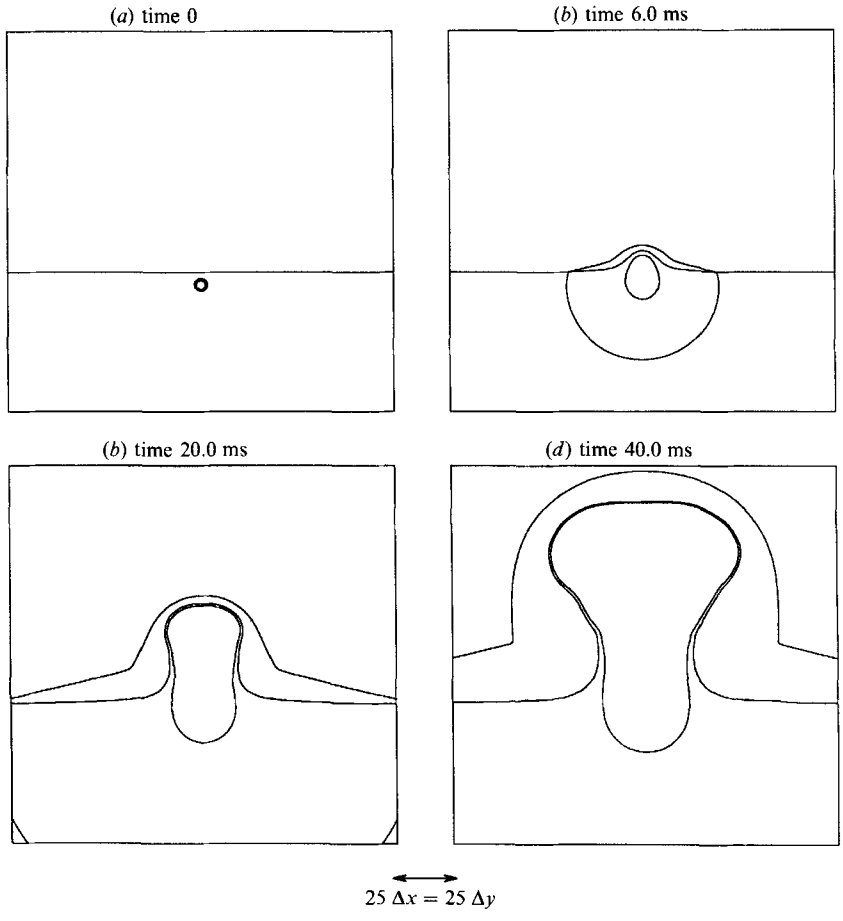

FIGURE 7. An underwater expanding shock wave diffracting through the water's surface. An expanding shock wave with an internal pressure of 10 Kbars and initial radius of 1 m is installed at a depth of 2 m below the water's surface. The external conditions are ambient at 1 atm. pressure and normal densities for the air and water. The boundary conditions are constant Dirichlet at the initial ambient values. The grid is 150×150.

expanding shock is 100 Kbar with the density and velocity of the reaction products initially set at 1.25 g/cc and 1.54 km/s respectively.

This simulation is qualitatively similar to that of the previous one, but the increased shock strength causes the simulation to evolve on a faster timescale.

6. Numerical considerations

These examples illustrate that the singularity structure from irregular wave interactions can be incorporated into the solution with the front-tracking method. Precisely knowing the positions of the fronts is a great aid for understanding the dominant features of the flow including when and how these features bifurcate. By explicitly taking into account the most singular aspect of the flow, the wave patterns, an accurate solution can be achieved with coarser mesh resolution than for shock capturing algorithms.

The wave patterns cause capturing algorithms difficulty for several reasons. A

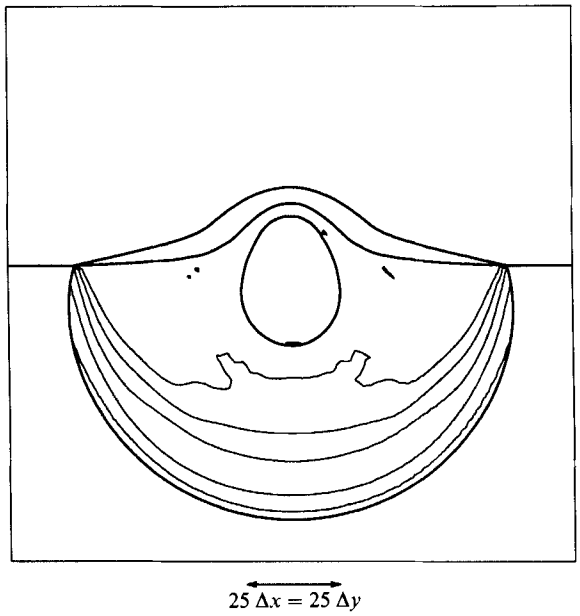

FIGURE 8. A blowup of figure 7(*b*) showing pressure contours scaled from 0.001–10 Kbars. The tracked interface is shown superimposed as a dark line over the pressure contours.

typical wave pattern, e.g. diffraction node, is the intersection of five waves. Most (high-order accurate) finite-difference schemes use quadrilateral meshes. The nodes must be smeared over many zones because of the difference in topology. Because the waves are independent degrees of freedom, front tracking is much less sensitive than (the usual directionally split) capturing schemes to the orientation of the waves with the numerical grid.

For shock capturing methods transients will occur when a wave crosses an interface between media with very different physical properties (such as density or compressibility) which take many zones to dissipate. This can be minimized by adjusting the grid such that the zone size in the normal direction on each side of the interface is proportional to their respective wave speeds. But this condition is frequently incompatible with other constraints such as limited mesh resolution. A large ratio of compressibility between materials results in a wave travelling many cells in the more compressible material during the time it takes a wave to travel one cell in the less compressible material. A similar difficulty occurs in resolving very thin rarefactions as occurred in the example in §4.1.

These difficulties are overcome with front tracking by storing multivalued states along the front and using Riemann solvers for propagating the front. Smearing out of nodes because of artificial viscosity and lack of sufficiently fine mesh resolution leads to difficulties in distinguishing between wave patterns such as the diffraction node and anomalous reflection, and thus make it difficult to understand the dominant features of the flow. In some cases, numerical schemes may not calculate the bifurcation of the wave patterns (such as diffraction to anomalous reflection) correctly and lead to qualitatively wrong flows.

Tracking a large number of waves becomes impractical. While it is important that the dominant waves be tracked, other weaker waves can be captured by the interior scheme with minimal loss in accuracy. This occurred in the example in §5. In the

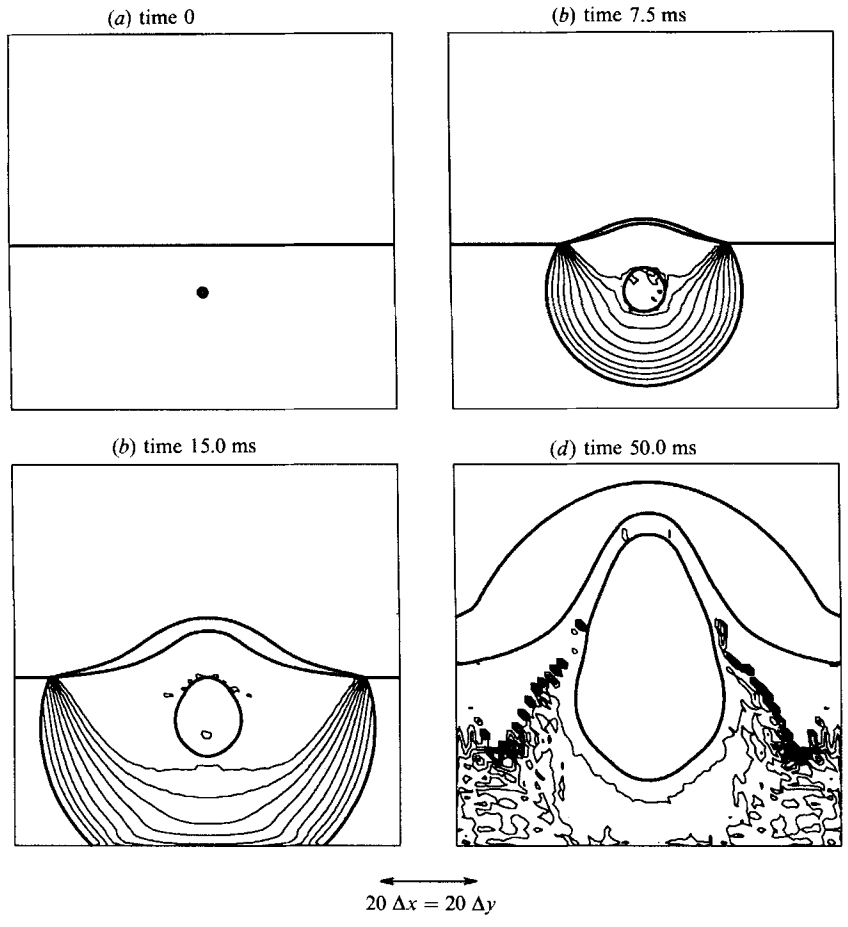

FIGURE 9. The same simulation as shown in figure 8 except an expanding shock wave with an internal pressure of 100 Kbars and initial radius of 1 m is installed 10 m below the water's surface. The figures show the tracked front as a dark line superimposed over $\log(1+P)$ contours scaled from the minimum and maximum pressure in each frame; (*a*) 0–10, (*b*) 0–5.4, (*c*) 0–3.2, (*d*) 0–0.36 Kbar. The grid is 60×60.

simulations of underwater explosions, for example, the edges of the reflected rarefaction produced by the diffraction of the shock through the surface were not tracked. The evolution of the transmitted air shock develops a kink or Mach node which was also not tracked. For the example in §4.2 we have preformed other calculations in which either the trailing edge or both edges of the rarefaction from the anomalous reflection nodes were not tracked. The loss in accuracy is discernible but the qualitative features of the flow are unchanged.

7. Summary

The qualitative features that dominate compressible fluid flow are shock, rarefaction and contact waves, and the elementary wave patterns which result from their interactions. We have discussed the mathematical framework that describes the wave patterns and explained the distinction between regular and irregular wave patterns. The regular wave patterns correspond to the solution of a Riemann

problem for two-dimensional steady supersonic flow. These Riemann problems are in the frame moving with the geometric node velocity. Irregular wave patterns occur when the solution to the Riemann problem fails to exist.

The smooth background flow causes the regular wave patterns to be quasi-steady; a slow variation in the strength and angle between the incoming waves which characterized the regular wave pattern. In fluid flows the irregular wave patterns typically arise when the quasi-steady regular wave patterns bifurcate into a composite of elementary wave patterns. A key point in describing the irregular wave patterns is to determine the node velocity.

We have illustrated this framework by describing in detail one of the irregular wave patterns, the anomalous reflection node. In this case the node velocity is determined by the condition that the flow behind the incident shock wave at the node is sonic. The anomalous reflection is the analogue of Mach reflection when the reflected wave is a rarefaction. A diffraction node with a reflected shock may bifurcate into a Mach node and a transmission node. Similarly, a diffraction node with a reflected rarefaction may bifurcate into an anomalous reflection node and a degenerate overtake node.

We have shown how the irregular wave patterns and the bifurcations of the regular wave patterns which generate them can be incorporated into a front-tracking algorithm for simulating fluid flow. This is illustrated with numerical calculations of a shock passing over a bubble and an underwater detonation.

Several open questions remain concerning the wave patterns that occur in fluid flow. These include a complete classification of all elementary wave patterns and a general description of the allowed bifurcations of elementary wave patterns into composite wave patterns. One example is the precursor wave pattern that occurs from a shock interaction at a slow–fast interface. In addition there is the problem of describing the scattering of nodes. Typically, this occurs when the interaction of a shock at the side boundaries of a medium generates nodes which propagate along the shock front. The nodes travelling along the shock front in opposite directions are bound to interact. These problems are of interest both from a physical and a mathematical point of view.

We would like to thank James Glimm for many helpful suggestions and his continued support of this work. J.W.G. was supported in part by the US Army Research Office, grant no. DAALO3-89-K-0017 and the National Science Foundation, grant no. DMS-8901884. R.M. was supported by the US Department of Energy.

REFERENCES

Abd-el-Fattah, A. M. & Henderson, L. F. 1978*a* Shock waves at a fast–slow gas interface. *J. Fluid Mech.* **86**, 15–32.

Abd-el-Fattah, A. M. & Henderson, L. F. 1978*b* Shock waves at a slow–fast gas interface. *J. Fluid Mech.* **89**, 79–95.

Artola, M. & Majda, A. 1989 Nonlinear kink modes for supersonic vortex sheets. *Phys. Fluids* A**1**, 583–596.

Ben-Dor, G., Dewey, J. M. & Takayama, K. 1987 The reflection of a plane shock wave over a double wedge. *J. Fluid Mech.* **176**, 483–520.

Ben-Dor, G. & Glass, I. I. 1979 Domains and boundaries of non-stationary oblique shock-wave reflexions. Part 1. Diatomic gas. *J. Fluid Mech.* **92**, 459–496.

Chang, T. & Hsiao, L. 1989 *The Riemann Problem and Interaction of Waves in Gas Dynamics.* John Wiley.

CHERN, I.-L., GLIMM, J., MCBRYAN, O., PLOHR, B. & YANIV, S. 1985 Front tracking for gas dynamics. *J. Comput. Phys.* **62**, 83–110.

COURANT, R. & FRIEDRICHS, K. O. 1948 *Supersonic Flow and Shock Waves*. Springer.

DEAR, J. P. & FIELD, J. E. 1988 A study of the collapse of arrays of cavities. *J. Fluid Mech.* **190**, 409–425.

GLIMM, J., ISAACSON, E., MARCHESIN, D. & MCBRYAN, O. 1981 Front tracking for hyperbolic systems. *Adv. Appl. Maths* **2**, 91–119.

GLIMM, J., KLINGENBERG, C., MCBRYAN, O., PLOHR, B., SHARP, D. & YANIV, S. 1985 Front tracking and two dimensional Riemann problems. *Adv. Appl. Maths* **6**, 259–290.

GLIMM, J. & MCBRYAN, O. 1985 A computational model for interfaces. *Adv. Appl. Maths* **6**, 422–435.

GLIMM, J. & SHARP, D. 1986 An S-matrix theory for classical nonlinear physics. *Foundations Phys.* **16**, 125–141.

GROVE, J. W. 1989 The interaction of shock waves with fluid interfaces. *Adv. Appl. Maths.* **10**, 201–227.

HAAS, J.-F. & STURTEVANT, B. 1987 Interaction of weak shock waves with cylindrical and spherical gas inhomogeneities. *J. Fluid Mech.* **181**, 41–76.

HENDERSON, L. F. 1966 The refraction of a plane shock wave at a gas interface. *J. Fluid Mech.* **26**, 607–637.

HENDERSON, L. F. 1988 On the refraction of longitudinal waves in compressible media. *Rep.* UCRL-53853. Lawrence Livermore National Laboratory.

HENDERSON, L. F. 1989 On the refraction of shock waves. *J. Fluid Mech.* **198**, 365–386.

HOLT, M. 1977 Underwater explosions. *Ann. Rev. Fluid Mech.* **9**, 187–214.

HORNUNG, H. 1986 Regular and Mach reflection of shock waves. *Ann. Rev. Fluid Mech.* **18**, 33–58.

JAHN, R. G. 1956 The refraction of shock waves at a gaseous interface. *J. Fluid Mech.* **1**, 457–489.

JONES, D., MARTIN, P. & THORNHILL, C. 1951 A note on the pseudo-stationary flow behind a strong shock diffracted or reflected at a corner. *Proc. R. Soc. Lond.* A **209**, 238–248.

KAMEGAI, M. 1986 Computer simulation of irregular surface reflection of an underwater shock wave. *Rep.* UCRL-96675. Lawrence Livermore National Laboratory.

LANDAU, L. & LIFSHITZ, E. 1959 *Fluid Mechanics*. Addison-Wesley.

LAX, P. 1957 Hyperbolic systems of conservation laws II. *Commun. Pure Appl. Maths* **10**, 537–556.

MADER, C. L. 1965 Initiation of detonation by the interaction of shocks with density discontinuities. *Phys. Fluids* **8**, 1811–1816.

MENIKOFF, R. 1989 Analogies between Riemann problem for 1-D fluid dynamics and 2-D steady supersonic flow. In *Contemporary Mathematics* (ed. W. Brent Lindquist) *Proc. 1988 Joint Research Conference on Current Progress in Hyperbolic Systems: Riemann Problems and Computations*, pp. 225–240. American Mathematical Society, Providence RI.

MENIKOFF, R. & PLOHR, B. 1989 Riemann problem for fluid flow of real materials. *Rev. Mod. Phys.* **61**, 75–130.

PICONE, J. M. & BORIS, J. P. 1988 Vorticity generation by shock propagation through bubbles in a gas. *J. Fluid Mech.* **189**, 23–51.

SCHWENDEMAN, D. W. 1988 Numerical propagation in non-uniform media. *J. Fluid Mech.* **188**, 383–410.

SKEWS, B. W. 1967 The perturbed region behind a diffracting shock wave. *J. Fluid Mech.* **29**, 705–719.

THOMPSON, P. 1971 A Fundamental derivative in gasdynamics. *Phys. Fluids* **14**, 1843–49.

WINKLER, K.-H., CHALMERS, J., HODSON, S., WOODWARD, P. & ZABUSKY, N. 1987 A numerical Laboratory. *Physics Today*, October, 28–37.